Available online at www.sciencedirect.com
SCIENCE DIRECT
Polymer 46 (2005) 6623–6632
polymer
www.elsevier.com/locate/polymer

# Microcellular foams from some high-performance composites

Hongliu Sun[a], James E. Mark[a,*], Seng C. Tan[b], N. Venkatasubramanian[c], Marlene D. Houtz[c], Fred E. Arnold[d], Charles Y-C. Lee[e]

[a]Department of Chemistry and the Polymer Research Center, The University of Cincinnati, Cincinnati, OH 45221-0172, USA
[b]Wright Materials Research Co., 1187 Richfield Center, Beavercreek, OH 45430, USA
[c]University of Dayton Research Institute, 300 College Park Drive, Dayton, OH 45469, USA
[d]Polymer Branch, Wright-Patterson Air Force Base, Dayton, OH 45433-7750, USA
[e]Directorate of Chemistry and Life Sciences, AFOSR/NL, Arlington, VA 22203-1977, USA

Available online 31 May 2005

**Abstract**

High-temperature composites were successfully prepared from aminated polysulfone, polyphenylsulfone, and a rod-like polymer polybenzimidazole (PBI). The single glass transition temperature $T_g$ and the absence of evidence for phase separation in scanning electron microscopy suggested that these systems formed so-called 'molecular composites'. The enhanced miscibility between the polymer pairs was probably due to hydrogen bonding interactions. Compared with the matrix polymers themselves, these composites have improved values of $T_g$ and thermal stability due to a synergistic effect upon incorporation of polybenzimidazole into the polymer matrices. Microcellular foams were successfully prepared from these composites. The foaming behavior and morphologies of the resulting composite foams were much more complicated than those of the pure polymers. In particular, they had unusual bimodal cell size distributions, and some open or partially open-cell structures.


*Keywords:* Polysulfone; Polybenzimidazole; Microcellular foams

## 1. Introduction

Since, Suh et al. at MIT proposed the idea of microcellular plastics and patented their first batch-foaming technique to prepare microcellular foams in the early1980s [1,2], there has been tremendous and still increasing interest in this area. These novel cellular materials, with cell sizes hundreds of times smaller and cell densities over ten thousand times higher than those of conventional plastic foams, can offer some unique properties that conventional foams cannot. One example is that of thin foams which are as thin as paper that could be used as coatings for data communication wires. Conventional foams cannot be used for this kind of applications, because the cells themselves are frequently larger than one or more dimensions in the products themselves. Over the past two decades, both fundamental and applied research and development have been extensively conducted in this area [5–11]. These researches have led to the better understanding of the physical phenomena governing the microcellular foaming process and the development of new foaming methods. These foaming processes have been successfully applied to many polymers, resulting in microcellular foams with cell sizes from less than1 μm to about 100 μm, depending on the polymer types and foaming conditions [5,12–14]. Very recently, Suh [4] reviewed the impact of microcellular plastics on industrial practice and academic research.

Relatively little has been done, however, to extend these microcellular foaming techniques to composites. Matuana et al. [15–17] studied the microcellular foaming behavior of PVC/wood–fiber composites using a batch-foaming process. Also, Bledzki [18] reported the production of polypropylene/wood–fiber composite microcellular foams in an injection molding process, and Wang et al. [8] investigated the foaming of polystyrene/liquid crystalline polymer composites. Similarly, Han and Zeng et al. [19,20] reported the preparation of polystyrene/clay nanocomposite foams by a supercritical $CO_2$ batch or continuous process. Very recently, Okamoto et al. [21,22] reported the cellular structure and alignment of silicate layers in polypropylene/

* Corresponding author. Tel.: +1 513 556 9292; fax: +1 513 556 9239.
*E-mail address:* markje@email.uc.edu (J.E. Mark).

0032-3861/$ - see front matter © 2005 Elsevier Ltd. All rights reserved.
doi:10.1016/j.polymer.2005.05.016

clay nanocomposite foams, and their results showed that the alignment of clay particles did help the cells to withstand the stretching force known to cause the breaking of the thin cell walls and thus have improved mechanical properties.

Molecular composites represent a relatively new concept in materials technology. They are defined as composites in which a rigid-rod polymer is molecularly dispersed in a flexible coil polymer matrix such that the rigid-rod molecules act as reinforcing elements [23–26]. The idea of molecular reinforcement is the translation of macroscopic fiber reinforcement to the molecular level. In molecular composites, the rigid molecular chains act as reinforcing fibers. The rigid-rod polymers have excellent mechanical properties and very high aspect ratios; in addition, there are no defects in a single molecular 'fiber' and, therefore, the theoretical strength due to the covalent bonds in the backbone chain can possibly be utilized for molecular-level reinforcement. In this sense, molecular fiber reinforcement is one approach to obtain the ideal properties of fiber-reinforced materials [27]. In addition to mechanical properties, the thermal properties of the molecular composite can also be expected to show large improvements over those of the polymer matrix. Most rigid-rod polymers have very high glass transition temperatures ($T_g$) or even no $T_g$ at all and exhibit excellent thermostability. Therefore, blending them into a flexible coil polymer matrix at the molecular level could result in high-performance composites with improved $T_g$ and thermostability compared to the matrix polymer. It would be of particular interest to expand some of these molecular composites into microcellular foams for structural applications. Having the rigid-rod chains aligned in the struts and walls of the foam could greatly improve its mechanical properties, such as compressive modulus and strength. Such foamed molecular composites should have superior thermal and mechanical properties, making them high-performance structural materials, and should have potential applications in a variety of fields, including military and commercial aircraft applications.

In our previous related studies [28–30], we found that chemically modified polysulfone, for example, sulfonated polysulfone (S-PSF) and carboxylated polysulfone (C-PSF) could form miscible composites with a rod-like polymer, polybenzimidazole (PBI) under certain conditions. The resulting molecular composites have enhanced thermostabilities and mechanical properties and can be readily converted into microcellular foams using a two-step batch foaming process based on dissolved carbon dioxide. In another report [31], poly(ether ketone ketone) (PEKK) was used as the thermoplastic matrix and polybenzobisthiazole (PBZT) as the rigid-rod polymer to form molecular composites. The foams processed from these PEKK/PBZT composites, though having higher densities and larger pore size than was expected, did show large improvements in mechanical and thermal properties relative to the pure PEKK foams. Recently, Krause et al. [32–35] also reported the production of some open-cell microcellular materials from polysulfone/polyimide molecular composites.

The present paper consists of two parts. In the first part, we discuss the formation of molecular composites from another type of chemically modified polysulfone, aminated polysulfone (N-PSF) and polyphenylsulfone (N-PPSF), with polybenzimidazole. In the second part, we investigate the effects of foaming conditions, such as foaming temperature, blend composition, $CO_2$ content, residual solvent etc. on the morphologies of some of the resulting microcellular composite foams.

## 2. Experimental

### 2.1. Materials

Samples of a polysulfone (Udel P-1700) (PSF) and a polyphenylsulfone (Radel R-5000) (PPSF) were kindly supplied by BP-Amoco. Values of their $T_g$ and density were, PSF: 185 °C and 1.34 g/cm$^3$, and PPSF: 220 °C and 1.29 g/cm$^3$. A sample of PBI powder with a mean particle size of 100 μm was purchased from the Goodfellow Corporation, Huntingdon, UK. All polymer samples were dried overnight at approximately 140 °C. Dimethylsulfoxide (DMSO), *N*,*N*-dimethylacetamide (DMAC) and *N*,*N*-dimethylformamide (DMF) were obtained from Aldrich and used as received. All other chemicals were purchased from Aldrich, and were employed in synthetic modifications of PSF and PPSF as described in the literature for amination [36,37]. Carbon dioxide (99.9%) was obtained from Wright Brothers Inc., Cincinnati, OH, USA.

### 2.2. Amination of polysulfone and polyphenylsulfone

Aminated polysulfone (N-PSF) and aminated polyphenylsulfone (N-PPSF) were prepared according to the procedure described by Guiver et al. [36,37]. First, polysulfone was lithiated by *n*-butyllithium at reduced temperatures (−50 to −70 °C) in tetrahydrofuran (THF) solution. The lithiated PSF was then converted to polysulfone azide intermediate by tosyl azide. Finally, the polysulfone azide was reduced to polysulfone (*ortho*-ether) diamine (referred to as aminated polysulfone, N-PSF in this study). For polyphenysulfone, the difficulty of dissolving the PPSF resin in THF required that the PPSF be first dissolved in DMAC or dichloromethane and then precipitated into ethanol. The resulting fine white powder could then be dissolved in THF in an ice bath to give a slightly gray solution, which was then used to make aminated polyphenylsulfone. The degree of substitution was 2.0 for both N-PSF and N-PPSF.

### 2.3. Preparation of N-PSF/PBI and N-PPSF/PBI molecular composites

PBI was first dissolved in DMSO/DMAC (1:1 v:v) to form a 2 wt% PBI solution; varying amounts of N-PSF and N-PPSF were then added into portions of the solution to form the desired compositions. The mixtures were stirred at 70 °C for about 8 h, after which the resulting clear solutions were poured into Petri dishes, and the solvent evaporated slowly at 90–100 °C. The resulting transparent films were vacuum-dried at 180–200 °C for about 24 h. Other composites were prepared as described elsewhere [28,29].

### 2.4. Preparation of microcellular foams

Microcellular foams were prepared from these composite films using the two-step batch process described elsewhere [38,39]. In brief, the composite films were saturated with $CO_2$ gas maintained at 5.5–5.7 MPa at room temperature. Upon saturation, the samples were removed from the pressure vessel and foamed in an oil bath maintained at the desired temperature.

### 2.5. Characterization of the molecular composite films and foams

Fourier transform infra-red (FTIR) spectra of the composite films (thin films with thickness about 50 μm) were recorded on a Bruker IFS 28 FTIR spectrometer. The morphologies of both the composite films and the corresponding microcellular foams were examined with a Hitachi S-4000 high-resolution scanning electron microscope (SEM). For these examinations, surfaces were generated by immersing the samples in liquid nitrogen prior to their fracture. Differential scanning calorimetry (DSC) was carried out under nitrogen at heating rate of 10 °C/min using a DSC-2910 apparatus, thermogravimetric analysis (TGA) with a 2950 TGA unit under air with a 10 °C/min heating rate, and thermal mechanical analysis (TMA) with TMA-2940 equipment in the fiber/film mode at 4 °C/min under nitrogen. All the instruments for thermal analysis were from TA Instruments.

## 3. Results and discussion

### 3.1. N-PSF/PBI and N-PPSF/PBI molecular composites

In their pristine forms, PSF and PPSF are not miscible with PBI, and form non-compatible binary systems [40,41]. PSF and PPSF, chemically modified by introducing sulfonate, amine, or carboxyl groups, however, were found to have enhanced miscibilities and formed compatible composites with PBI. In the present study, N-PSF and N-PPSF were blended with PBI in solution. Transparent films (0.2–0.5 mm thick) were obtained by solution casting and were characterized using FTIR, TMA, TGA and SEM.

#### 3.1.1. FTIR analysis

The FTIR spectra of N-PPSF, PBI and N-PPSF/PBI composites in the N–H stretching region (2600–3600 $cm^{-1}$) are shown in Fig. 1. Asymmetric and symmetric N–H stretching absorptions of the primary amine functionality occur around 3471 and 3373 $cm^{-1}$. This result confirms that amine groups were successfully grafted onto the PPSF chains. There is a weak band around 3221 $cm^{-1}$, which is possibly due to hydrogen bonding between N–H groups. There are four peaks clearly observable for pure PBI in this region [42]: 3401 $cm^{-1}$, which was attributed to the non-hydrogen bonded N–H groups; 3143 and 3183 $cm^{-1}$ assigned to self-associated hydrogen bonded N–H groups, and 3063 $cm^{-1}$ from aromatic C–H groups. The IR spectra are more complex for the composite systems, since both the rod and coil polymers contain N–H groups and their characteristic peaks overlap. With the addition of PBI, these two peaks from N–H of NPPSF were found to shift slightly to lower wavenumbers and a new, relatively broad peak centered around 3200 $cm^{-1}$ appeared, and moved to lower wavenumbers with increase of PBI content. This peak is probably due to the hydrogen bonding between the N-PPSF and PBI, which is presumably the reason for enhanced miscibility between the two components.

#### 3.1.2. TMA tests

Attempts to measure the values of $T_g$ for these molecular composites with DSC were not successful, but dimensional changes in TMA measurements did show very discernible

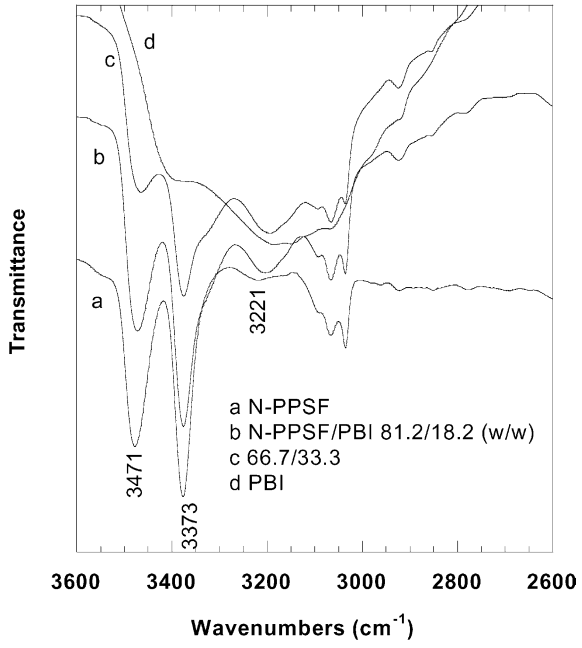


Fig. 1. FTIR spectra for (a) N-PPSF (b) and (c) N-PPSF/PBI composites, and (d) pure PBI.

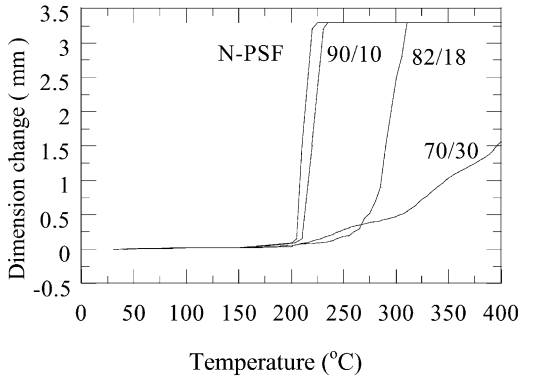


(A)

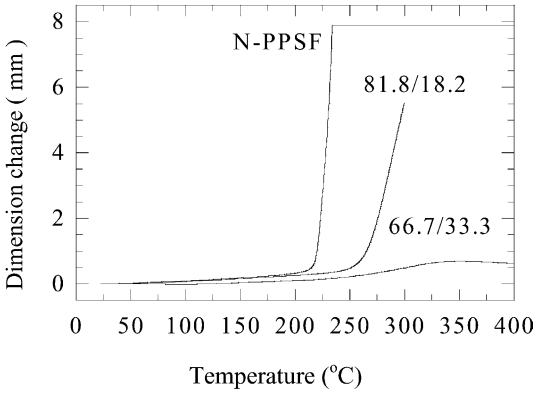


(B)

Fig. 2. TMA traces for (A) N-PSF/PBI, and (B) N-PPSF/PBI composites.

transitions, as shown in Fig. 2. The $T_g$ of N-PSF is 202 °C, which is approximately 16 °C higher than that for unmodified polysulfone. This is because the presence of amine groups increases the polarity of the polymer and increases $T_g$ through hydrogen bonding interactions. When PBI, which has a $T_g$ around 410 °C, was added to N-PSF, TMA results show a very obvious increase in $T_g$ upon increase in PBI content. At a low PBI content (10 wt%), the $T_g$ value slightly increased to 207 °C, but at a higher PBI content (18 wt%), it dramatically increased to 265 °C. For the 70/30 composition, there was a slight dimensional change from 200 to 300 °C. This change in this temperature range could possibly be caused by trace amounts of solvent (DMAC and DMSO) trapped in the composite films. Residual solvent could volatilize in the 200–300 °C range, plasticizing the composite, thus lowering their $T_g$. The residual solvent has significant effects on the morphologies of the composite foams (as discussed in the next part). Above 300 °C, the dimensions changed more markedly with temperature. Quite similar results were observed for N-PPSF/PBI composites, as shown in Fig. 2(B), except the $T_g$ values were higher. At high PBI content (33.3 wt%), there was no obvious dimensional change from 300 to 400 °C, as was also the case previously for S-PPSF/PBI composites [28]. This large increase in $T_g$ resulted from the synergistic effects due to PBI incorporation, and the single composition-dependent $T_g$ also indicated that the PBI was well dispersed into this modified PSF matrix to form molecular composites.

### 3.1.3. TGA measurements

These composites also exhibit improved thermo-oxidative stability relative to the matrix polymer, as shown by the TGA curves in air (Fig. 3). All the composites exhibited distinct two-stage decomposition profiles. The first stage degradation occurred around 360 °C, causing ~12% weight loss. This was mainly due to the loss of the pendant amine groups and some low molecular weight components. These materials degraded slowly with increase in temperature until it reached about 500 °C, at which point the N-PSF started to decompose quickly. For the composites, however, especially at higher PBI contents (20 and 30 wt%), this second stage decomposition was delayed and the final decomposition temperature increased to 580–610 °C (depending on the PBI content). For N-PPSF/PBI composites, decomposition profiles are somewhat different from the others. N-PPSF itself showed a broad two-stage

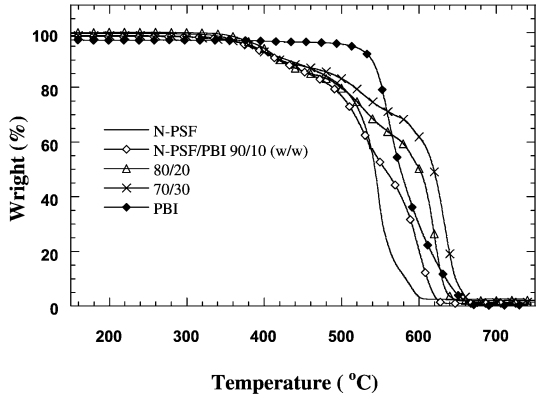


(A)

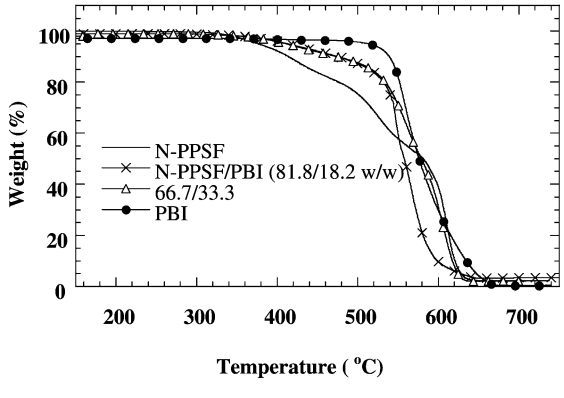


(B)

Fig. 3. TGA traces in air for (A) N-PSF/PBI, and (B) N-PPSF/PBI composites.

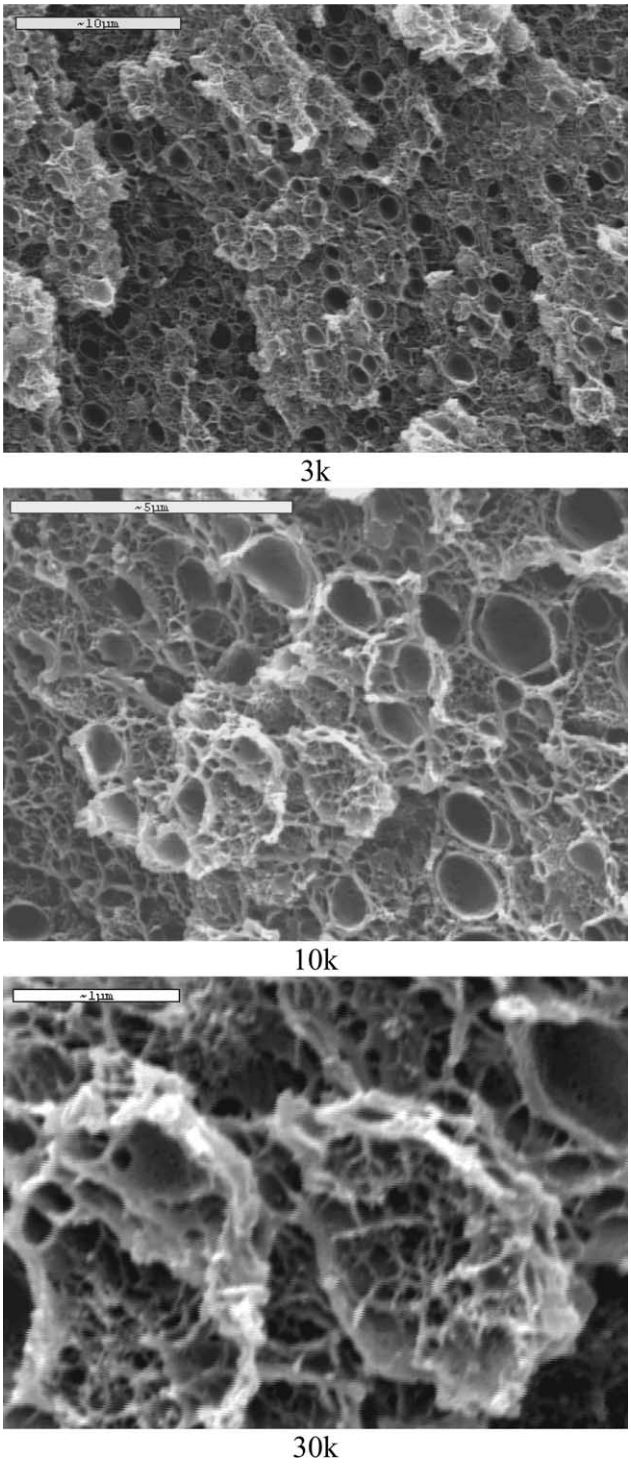


Fig. 4. SEM micrographs of S-PSF(Na)/PBI (90/10 w/w) foams at 180 °C foaming temperature (the numbers below specify magnifications).

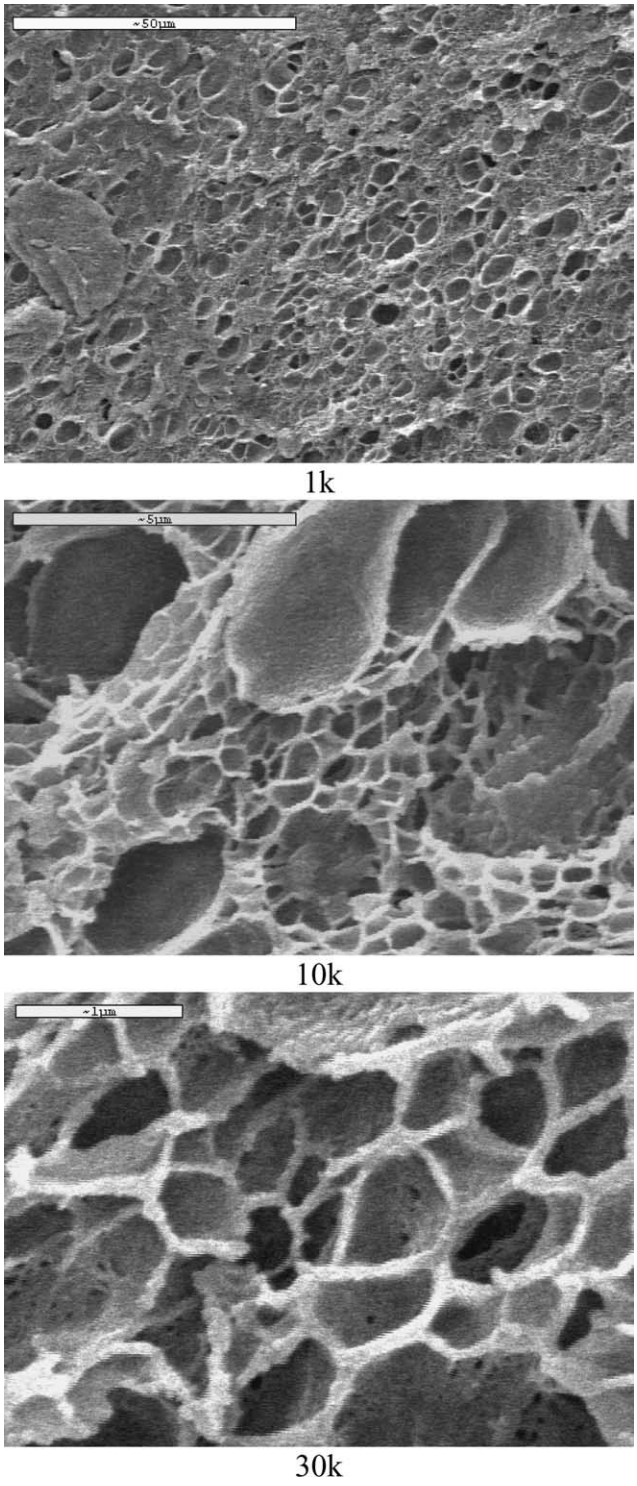


Fig. 5. SEM micrographs of S-PSF(Na)/PBI (90/10 w/w) foams at 230 °C foaming temperature.

degradation (first stage from 380 to 560 °C, second stage from 560 to 620 °C) as shown in Fig. 3(B). With the addition of PBI, the first-stage decomposition seemed somewhat suppressed, but the second stage did not change. Some additional experiments are needed to confirm this point.

### *3.2. Microcellular foams from molecular composites*

Some molecular composites from the present and previous work were successfully converted into microcellular foams using a two-step batch foaming process. Compared with the pure matrix polymers, PSF and PPSF,

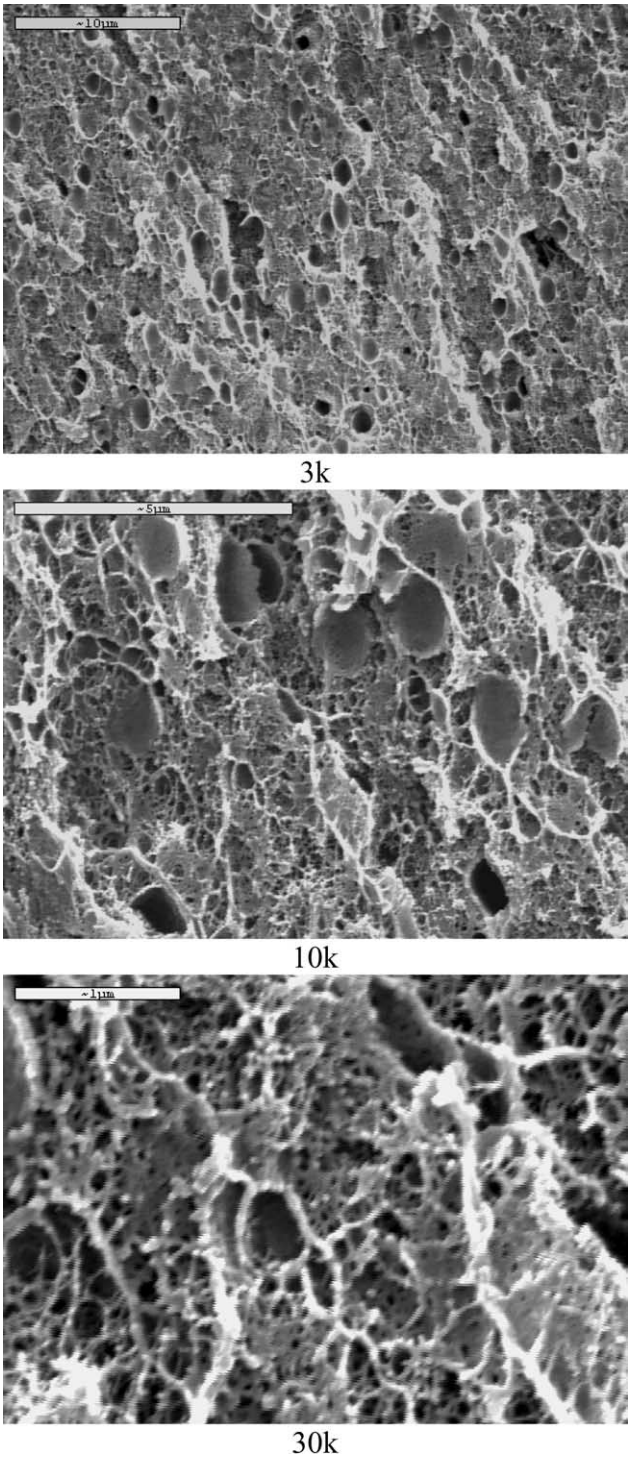


Fig. 6. SEM micrographs of S-PSF(Na)/PBI (80/20 w/w) foams at 180 °C foaming temperature.

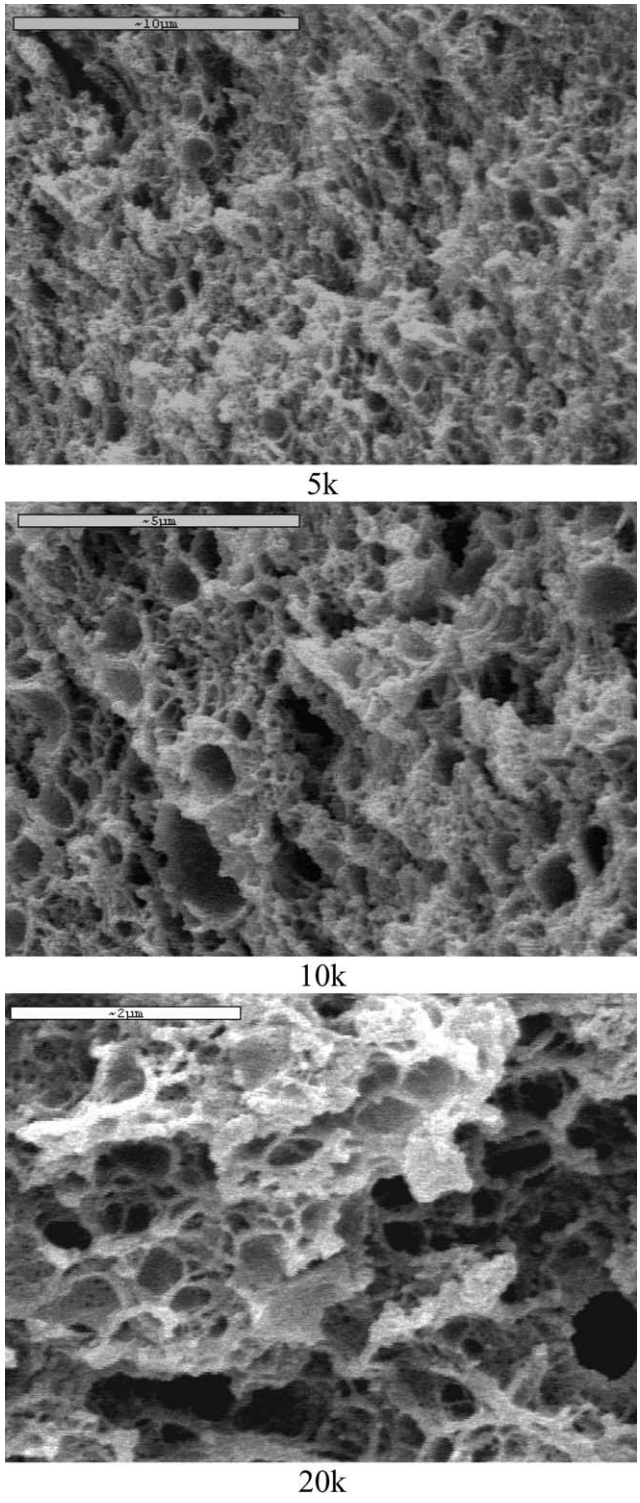


Fig. 7. SEM micrographs of S-PSF(Na)/PBI (80/20 w/w) foams at 230 °C foaming temperature.

the foaming behaviors of these solution-cast composite films were much more complicated, and the foaming process resulted in some materials with morphologies very different from the microcellular foams prepared from PSF and PPSF themselves.

### 3.2.1. Foaming temperatures and foaming times

The values of $T_g$ of pure PSF and PPSF are 185 and 220 °C, respectively. The absorption of $CO_2$ into a polymer can significantly lower its $T_g$, so the starting foaming temperature can be well below the $T_g$ of the pure polymer,

around 100 °C for PSF and 120 °C for PPSF [38,39]. The starting foaming temperature required by the composites is higher than that for pure PSF and PPSF. Because the sodium salt [28] composites (SPSF(Na)/PBI, S-PPSF(Na)/PBI, and N-PSF/PBI) have much higher values of $T_g$, and their chain segmental motions are highly restricted by strong specific interactions between the polymer chains, higher temperatures are required to soften the polymer and start the bubble nucleation. For example, for the S-PSF(Na)/PBI composite at 90/10 (w/w) composition, the starting foaming temperature increased to around 160 °C, and the 80/20 (w/w) composition gave only partially foamed structures at this temperature. Similar results were reported by Krause et al. [32] for polysulfone/polyimide (matrimid) composites; specifically, the starting foaming points shifted to higher temperatures with increasing matrimid content in the blend. In our experiment, attempts to fabricate foams from high PBI contents (30 wt%) in S-PPSF/PBI and N-PPSF/PBI composites at 230 °C foaming temperature were not successful. This was possibly due to the high $T_g$ and highly constrained chain motions in the composites. Another possible explanation is that at high PBI contents, there is some phase separation in the composites and the rigid-rod chains might act as barriers to the absorption of $CO_2$ and thus complicate the foaming process.

Foaming time used in our experiments was dependent on the thickness of the samples. For pure PSF and PPSF, the sample thickness was 1.5 mm and the foaming time ranged from 30 s to 2 min. For these solution-cast composite films, the thickness varied from 0.2 to 0.6 mm, so the foaming time used were 5–15 s.

### 3.2.2. Morphologies of the composite foams

The PSF and PPSF foams have well-defined closed-cell, polyhedral cell structures. The average cell size increased with the foaming temperature and was about 6.3 and 4.5 μm for PSF and PPSF foams at a foaming temperature around 180 °C [38,39]. The morphologies of composite foams are significantly different from those of PSF and PPSF foams. In general, the average cell size of the composite foams is smaller than those of foams from pure polymer matrices, and composite foams have unusual bimodal cell size distributions. They can also have open or partially open cell structures, which are dependent on the foaming temperature, composition, residual solvent, microphase separation, etc. Typical SEM micrographs at different magnifications of the microcellular foams prepared from S-PSF(Na)/PBI 90/10 (w/w) are presented in Fig. 4. At various magnifications, the SEM micrographs revealed very interesting microstructures. At a relatively low magnification (3$k$, $k=1000$), the micrograph showed typical microcellular structures with average pore sizes around 2 μm. When the magnification was increased to 10$k$, the micrograph revealed a clearly bimodal cell structure: the large cells were about 2 μm, the small cells about 0.1–0.3 μm, and both the large and small cells were relatively uniform among themselves. When the magnification was further increased to 30$k$, the SEM micrograph showed that these small cells were connected to each other to form open-cell structures. This interesting bimodal cell size distribution and the novel occurrence of open-cell structures are seldom seen with microcellular plastics. Arora et al. [43] reported bimodal cell structures, however, for microcellular polystyrene foams. In their experiment, the bimodal foam was generated by reducing the $CO_2$ pressure in two stages. In the first stage, the $CO_2$ pressure was dropped from 41.4 to 27.6 MPa, resulting in phase separation leading to the formation of large cells. During the second depressurization stage, a second set of cells was nucleated and grown within the walls of the first set, resulting in bimodal cell-size distributions. However, the material produced in their process was a closed-cell foam. In our experiment, this bimodal structure was caused by the phase separation occurring during the preparation of the composite films and

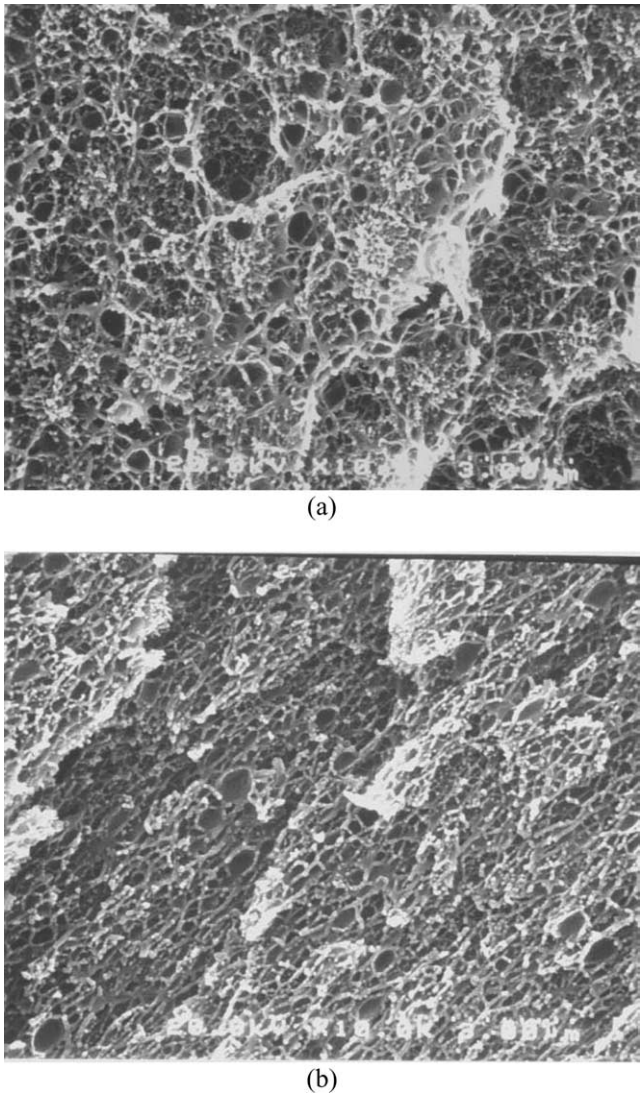

Fig. 8. SEM micrographs of S-PPSF(Na)/PBI composite foams at 180 °C foaming temperature, (a): 90/10 (w/w) composition, (b): 80/20 (w/w).

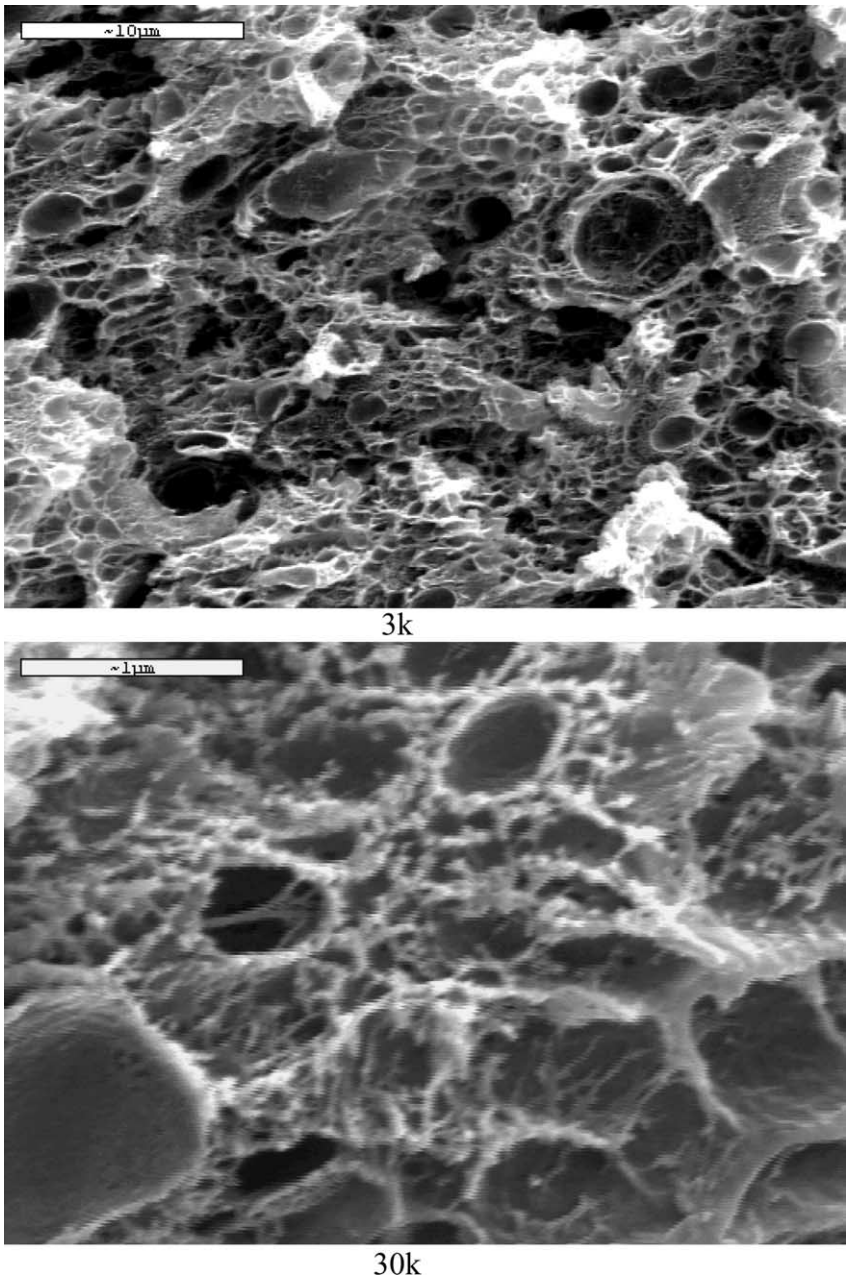


Fig. 9. SEM micrographs of N-PSF/PBI (90/10 w/w) composite foams at 180 °C foaming temperature (the thin films were not post-dried and the saturation time was 70 h).

the subsequent foaming process. The DMAC and DMSO solvents used in the film preparation have high boiling points (166 and 189 °C), making complete removal of solvent from the composites quite difficult. Trace amounts of solvent trapped in the composite films could volatilize and plasticize the composites, thus causing a small extent of phase separation during the evaporation of the solvent at high temperatures (200 °C), as can be seen from the randomly distributed sparse dots (about 20–40 nm) in the SEM micrographs [28]. In the foaming stage, the absorbed $CO_2$ could plasticize the composites and decrease the $T_g$ well below that of the original composite. The phase separation then occurred when the $CO_2$-saturated sample was heated to a high temperature during the foaming process.

This phase separation caused the occurrence of bimodal distributions of cell size. Specifically, the PSF-rich domains, which have lower $T_g$, resulted in large cells, while the PBI-rich parts formed small cells. The open-cell structure was caused by the residual solvent, which can deteriorate the cell walls during the expansion of the polymer and result in the interconnected cells. This observed 'cell bursting' is consistent with a report by Krause et al. [32–35] that open-cellular polysulfone and polysulfone/polyimide

composites microporous materials could be prepared using trace amounts of solvent as 'pore openers'. They also found when the $CO_2$ concentration was above some critical value, bicontinuous nanoporous films were obtained.

When the foaming temperature was increased to 230 °C, the cell size increased to 4–5 μm for the large cells and to around 1 μm for the small cells, as is shown in Fig. 5. This is consistent with the fact that higher foaming temperatures generally give rise to larger cell sizes. But the open-cell structure was not as evident as in the 180 °C foamed sample, possibly because the amount of residual solvent in this sample was smaller. This result suggests that the extent of openness could be controlled by the amount of residual solvent, as was confirmed with the other composite foams in the following discussion.

Composition can also affect foam morphology. SEM micrographs of microcellular foams from the S-PSF(Na)/PBI 80/20 (w/w) composites at 180 °C foaming temperature are shown in Fig. 6. Again, there is a bimodal, open-cell structure with the large cells slightly decreased in size, but the small cells significantly smaller than those from the 90/10 composition. Also, the cell structures became more open, which was most probably caused by more residual solvent being present. Fig. 7 presents the micrographs of foam at an 80/20 composition foamed at 230 °C. Compared with the results in Fig. 6 (same composition, lower foaming temperature), the large cells seem slightly smaller, but the small cells seem larger. This is possibly related to the extent of phase separation in the composites generated during the film preparation. There are many parameters that can cause phase separation in the composites that even minor differences in the experimental conditions can affect the foaming process. Compared with the results in Fig. 5 (same foaming temperature, smaller PBI content), both the small and large cell sizes decreased with increasing PBI content.

The micrographs of the S-PPSF(Na)/PBI (90/10 and 80/20 w/w) composites foamed at 180 °C are shown in Fig. 8. For the S-PPSF(Na)/PBI system, the bimodality of size distribution was not as marked as in the case of the S-PSF(Na)/PBI composites. This suggested that there was less phase separation in these composites. The foams had partial open-cell structures and the cell sizes were around 0.2–0.5 μm. With increase in PBI content, the cell sizes were found to decrease slightly.

N-PSF/PBI (90/10 w/w) composite foams gave some particularly interesting morphologies that were significantly different from those of the other composite foams. When the thin films (about 0.2 mm in thickness) were dried at 190 °C and saturated in $CO_2$ for a longer time (70 h), the resulting foams had very similar morphologies to the S-PSF(Na)/PBI foams, specifically, bimodal size distributions and open-cell structures, as shown in Fig. 9. But when the films were relatively thick (0.5–0.6 mm) and further dried at higher temperature (240 °C) after the usual vacuum drying, and the saturation time was about 20–24 h, the resulting foams had closed-cell structures, as was observed for the pure PSF foam, but the cell densities were much lower. Fig. 10 presents a typical SEM micrograph of these kinds of foams. At 230 °C foaming temperature, the resulting foams had a very uniform closed-structure with average cell sizes about 3–4 μm. Apparently, the post-drying process not only helped to get rid of the residual solvent but could also possibly cause some chemical reactions to occur or promote

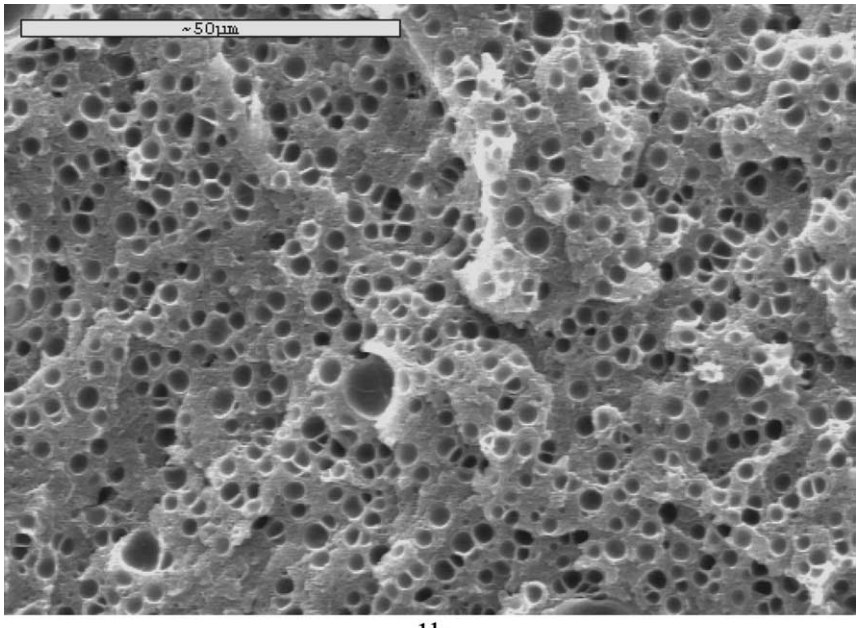


Fig. 10. SEM micrograph of N-PSF/PBI (90/10 w/w) composite foams at 230 °C foaming temperature (the thick films were post-dried and the saturation time was 20 h).

crosslinks between the N-PSF and PBI chains. These factors could consequently affect the composite foaming behavior, leading to the closed-cell foam structure. The short saturation time caused a lower $CO_2$ concentration in the composites, and resulted in lower cell densities in the foams.

In summary, microcellular foams were successfully prepared from high-performance molecular composites. Composite foaming behaviors were very complicated, and many variables were found to affect the foaming process and foam morphology; as a result, more investigations will be required to attain a better understanding of these phenomena. These novel microcellular foams with partial-open-cell structures might well have some applications as high-performance structural materials or as membranes.

## 4. Conclusions

Chemical modifications of polysulfone and polyphenylsulfone chain by introducing functional groups, such as sulfonate, or amine, were shown to significantly enhance their miscibility with the rod-like polybenzimidazole. PBI was found to be well dispersed in the modified PSF matrices, down to the nanoscale and possibly even at the molecular level to form molecular composites. These composites exhibit increased glass transition temperatures and improved thermo-oxidative stabilities. Microcellular foams with bimodal cell size distributions ranging from 5 to 0.2 μm, and open or partially open-cell structures were also successfully fabricated from these high performance composites.

## Acknowledgements

It is a pleasure to acknowledge the financial support provided by the Air Force Office of Scientific Research (Directorate of Chemistry and Materials Science) through Grant F49620-98-1-0319. H. Sun also appreciates the helpful discussions he had with Dr M. D. Guiver of the Institute for Chemical Process and Environmental Technology, National Research Council, Ont., Canada.

## References

[1] Martini JE, Waldman FA, Suh NP. SPE Tech Pap 1982;1:674.
[2] Martini JE, Suh NP, Waldman FA. US Patent 4,473,665; 1984.
[3] Nadis S. Bubbles by the billions. MIT's technology review. vol. 100 1998 Cambridge, MA: MIT Press p. 11.
[4] Suh NP. Macromol Symp 2003;201:187.
[5] Park CB. In: Lee ST, editor. Foam extrusion. Lancaster, PA: Technomic Publishing Company; 2000. p. 263.
[6] Baldwin DF, Park CB, Suh NP. Polym Eng Sci 1996;36:1425.
[7] Colton JS, Suh NP. Polym Eng Sci 1987;27:493.
[8] Wang J, Cheng X, Yuan M, He J. Polymer 2001;42:8265.
[9] Arora KA, Lesser AJ, McCarthy TJ. Polym Eng Sci 1998;38:2055.
[10] Goel SK, Beckman EJ. Polym Eng Sci 1994;34:1137.
[11] Goel SK, Beckman EJ. Polym Eng Sci 1994;34:1148.
[12] Baldwin DF, Tate DE, Park CB, Cha SW, Suh NP. J Jpn Soc Polym Proc (Seikei-kakou) 1994;6:187.
[13] Baldwin DF, Tate DE, Park CB, Cha SW, Suh NP. J Jpn Soc Polym Proc (Seikei-kakou) 1994;6:245.
[14] Kumar V, Weller JE. Microcellular foams. In: Khemani KC, editor. Polymeric foams. ACS symposium series 669. Washington, DC: American Chemical Society; 1997.
[15] Matuana LM, Park CB, Balatinecz JJ. Polym Eng Sci 1997;37:1137.
[16] Matuana LM, Park CB, Balatinecz JJ. Polym Eng Sci 1998;38:3862.
[17] Matuana LM, Park CB, Balatinecz JJ. J Cell Plast 1996;32:449.
[18] Bledzik AK, Faruk O. SPE ANTEC Tech Pap 2002;2:1897.
[19] Han X, Zeng C, Lee LJ, Koelling KW, Tomasko DL. SPE ANTEC Tech Pap 2002;2:1915.
[20] Zeng C, Han X, Lee LJ, Koelling KW, Tomasko DL. SPE ANTEC Tech Pap 2002;2:1504.
[21] Nam PH, Maiti P, Okamoto M, Kotaka T, Nakayama T, Kokada M, et al. Polym Eng Sci 2002;42:1907.
[22] Okamoto M, Nam PH, Maiti P, Kotaka T, Nakayama T, Kokada M, et al. Nano Lett 2001;1:503.
[23] Helminiak TE, Benner CL, Husman GE, Arnold FE. US Patent 4,207,407; 1980.
[24] Wang CS, Goldfarb IJ, Helminiak TE. Polymer 1988;29:825.
[25] Takayanagi M, Ogata T, Morikawa M, Kai T. J Macromol Sci Phys 1980;B17:591.
[26] Takayanagi M, Goto K. J Appl Polym Sci 1984;29:2547.
[27] Parker G, Hara M. Polymer 1997;38:2701.
[28] Sun H, Venkatasubramanian N, Houtz MD, Mark JE, Tan SC, Arnold FE, et al. Colloid Polym Sci 2004;282:502.
[29] Sun H, Mark JE, Tan SC, Venkatasubramanian N, Houtz MD, Arnold FE, et al. Nonlinear Opt Quantum Opt 2004;31:1.
[30] Sun H, Mark JE, Venkatasubramanian N, Houtz MD, Tan SC, Arnold FE, et al. J Macromol Sci Part A—Pure Appl Chem 2004;A41: 981.
[31] Tan SC, Bai Z, Sun H, Mark JE, Arnold FE, Lee CYC. J Mater Sci 2003;38:4013.
[32] Krause B, Diekmann K, van der Vegt NFA, Wessling M. Macromolecules 2002;35:1738.
[33] Krause B, Mettinkhof R, van der Vegt NFA, Wessling M. Macromolecules 2001;34:874.
[34] Krause B, Sijbesma HJP, Muenueklue P, van der Vegt NFA, Wessling M. Macromolecules 2001;34:8792.
[35] Krause B, Boerrigter ME, van der Vegt NFA, Strathmann H, Wessling M. J Membr Sci 2001;187:181.
[36] Giuver MD, Robertson GP. Macromolecules 1995;28:294.
[37] Giuver MD, Robertson GP, Foley S. Macromolecules 1995;28:7612.
[38] Sun H, Mark JE. J Appl Polym Sci 2002;86:1692.
[39] Sun H, Sur GS, Mark JE. Eur Polym J 2002;38:2373.
[40] Chung TS, Click M, Power EJ. Polym Eng Sci 1993;33:1042.
[41] Chung TS. Polym Eng Sci 1993;34:428.
[42] Deimede V, Voyiaatzis GA, Kallitsis JK, Qingfeng L, Bjerrum NJ. Macromolecules 2000;33:7609.
[43] Arora KA, Lesser AJ, McCarthy TJ. Macromolecules 1999;32:2562.